INTERNATIONAL JOURNAL OF HYDROGEN ENERGY 42 (2017) 9482–9492

Available online at www.sciencedirect.com

ScienceDirect

journal homepage: www.elsevier.com/locate/he

Ni/CeO_2–MgO catalysts supported on stainless steel plates for ethanol steam reforming

José A. Santander[*], *Gabriela M. Tonetto*, *Marisa N. Pedernera*, *Eduardo López*

Planta Piloto de Ingeniería Química PLAPIQUI (UNS-CONICET), Camino La Carrindanga Km 7, CC 717, CP 8000, Bahía Blanca, Argentina

ARTICLE INFO

Article history:
Received 22 October 2016
Received in revised form
22 March 2017
Accepted 23 March 2017
Available online 11 April 2017

Keywords:
Renewable hydrogen
Structured reactors
Steam reforming
Cerium oxide
Nickel

ABSTRACT

Ni/CeO_2–MgO catalysts on powder form and supported on stainless steel plates were prepared, characterized and tested towards hydrogen generation via the steam reforming reaction of ethanol. The structured catalyst was prepared by the dip-coating technique. The coatings obtained over the stainless steel plates were homogeneous and retained their integrity after the reaction experiences. The samples were characterized by SEM, TEM, XRD, ICP-AES, TPR, OSC and N_2 adsorption–desorption measurements. Catalysts presented very good stability under reaction conditions for 16 h on-stream, without showing a significant variation in the activity or product distribution. The structured catalysts presented similar activities and selectivities respect to those of the powder, whereby the deposition method did not modify the catalytic properties of the particulate material. The presence of the AISI 430 stainless steel substrate also had not a significant influence on the performance of the deposited material.

Introduction

Hydrogen has been considered one of the few long-term sustainable clean energy carriers. It shows a huge capacity of reducing environmental contamination due to the fact that only water vapor is emitted as by-product during the oxidation process. Moreover, vehicles operating on hydrogen can significantly reduce the dependence on fossil fuels [1]. One of the basal pillars in which the use of hydrogen is envisaged is the employment of renewable and non-polluting feedstocks for its generation. Feeds to the H_2 generator consisting on biomass-derived liquids have caught great interest since an almost-closed CO_2 cycle can be achieved, diminishing consequently the net emission of greenhouse gases. Specifically, bioethanol appears as an appealing raw source based on its high H_2 content, wide availability and advantageous safety concerns in its handle and storage [2].

Hydrogen generation by catalytic steam reforming of renewable fuels (e.g., bioethanol, bio-oil) has been pointed as attractive for its implementation at low/medium scales as decentralized production units or on-board or on-demand facilities [3–5]. The use of structured reactors supposes a wide number of advantages when compared to conventional packed-bed systems. Among them, it's worth mention a reduction in pressure drop across the reactor (roughly by two/three orders of magnitude), enhanced resistance to plugging due to depositions (e.g., coke), simpler scale-up, flexibility in the reactor design and eventually catalyst replacement and heat transfer improvements [6–8]. Regarding the last item,

* *Corresponding author*. Fax: +54 291 4861600.
E-mail addresses: jsantander@plapiqui.edu.ar (J.A. Santander), gtonetto@plapiqui.edu.ar (G.M. Tonetto), mpedernera@plapiqui.edu.ar (M.N. Pedernera), elopez@plapiqui.edu.ar (E. López).
http://dx.doi.org/10.1016/j.ijhydene.2017.03.169
0360-3199/

structured systems with characteristic dimensions in the order of millimeters o ever lower allow the operation with high area/volume ratios and enhanced heat & mass transfer coefficients, which leads to compact and efficient reaction units with precise control of the process conditions and improvements in safety operation [9–11]. Ethanol steam reforming (ESR) has been reported in the literature using structured catalysts and structured reactors and leading to high performances in terms of hydrogen production [5,12,13].

Ceramic and metallic materials are commonly used as catalysts carriers to build up structured reactors. Metallic substrates show some advantages over ceramics; some of them being better heat transfer characteristics, enhanced mechanical resistance, lower pressure drops due to the possibility of using thinner walls and consequently higher void fractions [14]. Among diverse options, ferritic stainless steel appears as an appealing choice since it presents strength, ductility, and corrosion resistance [15]. This material is only scarcely found along the literature as a structured catalyst substrate [16]. It is readily available in thin wall thickness; it is cheap and it shows suitable mechanical properties towards the carriers manufacture.

The catalysts employed in the ethanol reforming reaction should show adequate levels of activity and selectivity but, moreover, the catalysts should guarantee stability in terms of constant performance over time-on-stream. In addition, low-cost catalysts are obviously preferred. Although catalysts based on noble metal are efficient in ethanol steam reforming towards hydrogen production, their cost is significantly high. Ni catalysts are pointed as excellent candidates for ESR due to the capacity of this metal to activate C–C and C–H bonds and the low cost of Ni [17]. However, catalysts based on Ni show a tendency to deactivation under the reaction conditions due to carbon deposition and sintering of the Ni particles [18]. In this context, and among different strategies to mitigate this problem, a possible choice is the use of a support capable of oxidizing the deposited carbon.

The use of cerium oxide as support to carry out ESR has been extensively reported based on its oxygen storage capacity (OSC). The oxygen from the CeO_2 lattice takes part on the oxidation of the carbonaceous species over the catalyst surface [19,20]. On the other hand, the presence of Ce contributes in the dissociative adsorption of water from the reacting media giving place to –O and –HO species, which are transferred to the carbon on the surface to form CO, H_2 and CO_2, enhancing consequently the stability and hydrogen yield [21]. Modifications of CeO_2 with the addition of Mg are reported to improve the OSC and oxygen mobility in the support, leading to lower rates of carbon accumulation [19].

The present contribution focuses on the study of nickel catalysts supported over CeO_2–MgO, both in powder form or structured catalysts of AISI 430 corrugated metal sheets, for hydrogen production via ethanol steam reforming.

Materials and methods

Powder catalyst preparation

Powder catalysts were obtained in a first step, prior the deposition over the metallic structured substrates. The co-precipitation method was adopted here to synthesize the CeO_2–MgO support. To these ends, magnesium and cerium chloride aqueous solutions were employed with a Ce:Mg molar ratio of 0.85:0.15. In a typical procedure, the desired amounts of $CeCl_3 \cdot 7H_2O$ (Aldrich, 99.9%) and $MgCl_2 \cdot 6H_2O$ (Cicarelli, 99%) precursors were dissolved under stirring in 100 cm^3 of deionized water at room temperature. A hydrogen peroxide solution 30% (w/w) in H_2O was added at a H_2O_2:Ce = 1:3 molar ratio and the coprecipitation was conducted under vigorous stirring with the addition of 100 cm^3 of an 0.3 M aqueous $(NH_4)_2CO_3$ solution. The pH was adjusted to 9.5 by using an ammonium hydroxide solution 25% NH_3 in H_2O. The achieved precipitate was then repeatedly washed to eliminate the remaining Cl^- ions. The powder was then dried at 120 °C for 12 h and calcined in air at 550 °C for 4 h. The support is denoted as CeMg. Finally, the desired amount of active phase (Ni, 7 wt.%) was loaded over the CeO_2–MgO support by incipient wetness impregnation by means of an aqueous $Ni(NO_3)_2 \cdot 6H_2O$ solution. The prepared catalyst is referred as Ni/CeMg. The latter sample after the reaction test was denoted as Ni/CeMg–R.

Structured catalyst preparation

Structured catalysts in the form of corrugated pieces were prepared from AISI 430 stainless steel sheets of 100 μm thickness. For these purposes, plain rectangular sheets of L × W = 50 × 28 mm were first repeatedly washed and treated with acetone. By using a home-made device consisting of two cogwheels mechanized in Nylon, the plain sheets were corrugated giving place to pieces of L × W × H = 50 × 27 × 1.1 mm, with parallel channels of 0.69 mm equivalent diameter. In order to generate roughness in the metal surface aiming to the subsequent catalyst deposition, samples were treated in chromatographic air at 940 °C for 60 min. These treatment conditions were selected following previous reports from our group [16].

The corrugated substrates were later coated with the catalyst by means of the dip-coating technique. For that purpose, an aqueous suspension with 22.5 wt.% of CeMg support was prepared. In order to increase the coating adherence and to improve the stability of the catalytic suspension, colloidal SiO_2 (Ludox TMA, Aldrich) was added as a binder with a SiO_2:support mass ratio of 1:10. The stainless steel structures were dipped and withdrawn from the suspension, the excess material being removed by air blowing. Then the samples were dried at 120 °C for 30 min. The procedure was repeated until the desired loading of CeMg support was achieved over the substrates (180–200 mg). Finally, the samples were calcined at 500 °C for 2 h in air. The active phase Ni was incorporated by immersion in an aqueous solution of $Ni(NO_3)_2 \cdot 6H_2O$, followed by drying at 80 °C for 12 h and calcination at 550 °C for 3 h. This procedure was repeated until a Ni loading of 7 wt% was reached. The structured catalyst is denoted as SS-Ni/CeMg. After the reaction test, the latter sample is referred as SS-Ni/CeMg–R.

Catalyst characterization

The morphology of the substrate surface was examined by scanning electron microscopy (SEM) on a JEOL JSM 35CF microscope.

Transmission electron microscopy (TEM) images were obtained using a JEOL 100 CXII equipment operating at 100 kV. The studies were carried out using magnifications between 100000× and 270000×. Prior to the analysis, the samples were dispersed in ethanol using a sonicator.

The adherence of the catalytic layer deposited over the metallic substrates was tested by the ultrasonic method. The corrugated samples were immersed in 30 cm^3 of diethyl ether and subjected to an ultrasonic bath for 30 min in a Cole Parmer 8892E-MT (47 kHz, 105 W) instrument at room temperature. Then, the solvent was evaporated. The weight of each sample was measured before and after the ultrasonic treatment to determine the adherence, which was calculated as the percentage ratio of the amount of coating material retained to the amount of coating material present before the treatment.

The metal content was determined by inductively coupled plasma (ICP-AES) on a Shimadzu 9000 simultaneous atomic emission spectrometer.

Specific surface areas were determined by N_2 adsorption at 77 K, using the multipoint Brunauer–Emmett–Teller (BET) analysis method with a Quantachrome NOVA 1200e apparatus.

X-Ray diffraction (XRD) patterns were obtained using a Philips PW1710 diffractometer, with a monochromatic Cu-Kα source operating at 45 KV and 30 mA. The XRD profiles were recorded with 0.02° (2θ) steps over 10–80° angular range and 1 s counting time per step.

Thermogravimetric analyses were performed from room temperature up to 800 °C, at 10 °C/min in air, using a Discovery TGA thermogravimetric apparatus.

Temperature-programmed reduction (TPR) was carried out in a conventional apparatus equipped with a thermal conductivity detector (TCD). The samples were pretreated in flowing air at 300 °C for 30 min, followed by flowing Ar treatment for 30 min at the same temperature. After cooling to 25 °C, the temperature was raised to 600 °C at a rate of 10 °C/min in a 5% H_2/Ar flow (50 cm^3/min).

OSC measurements were carried out using a Micromeritics AutoChem II 2920 Catalyst Characterization System coupled to a Pfeiffer Quadstar mass spectrometer. Prior to the analysis, a cleaning pre-treatment with flowing air was performed from room temperature to 400 °C at a 10 °C/min heating rate for 30 min and a flow rate of 50 cm^3/min. After an argon purge at 400 °C, CO pulses (0.5 cm^3, measured at 1 atm and 20 °C) were injected every 6 min at constant temperature.

Catalytic tests

Due to the different morphology of the prepared catalysts, two different experimental setups were selected to study their performance in the ethanol steam reforming reaction. Powder samples were disposed into a fixed bed reactor consisting of a quartz tube of 4 mm inner diameter. Typically, 30 mg of catalyst were loaded, retained between quartz wool plugs.

On the other hand, corrugated structures were tested in an isothermal flat-bed reactor. This unit consists of two stainless steel halves that give place upon union to a central chamber of 28 mm wide by 250 mm long by 3 mm height (see Fig. 1). This chamber can accommodate up to three sections of catalysts (maximum length = 50 mm each). K-type thermocouples contact the catalysts at the middle of each section. The reactor has also a sliding thermocouple to measure an axial temperature profile and detect possible occurrence of hot/cold spots. Side ports located in the outlet of each catalyst section allow determining the composition of the reaction products at different axial positions. Reactants flow uniformity was achieved by flow distributors placed in the inlet section of the chamber.

The heat supply required for the reforming reaction is provided by an electric furnace inside which both reactors were placed. A solution of ethanol:water in molar ratio 1:6 (i.e., S/C = 3) is supplied by means of a syringe pump. Additionally, N_2 used as carrier is fed by a mass flow controller. The liquid feed is vaporized at 160 °C prior to being mixed with the carrier. After condensation of the excess water at the reactor outlet, the gaseous reaction products were analyzed with an HP Agilent 4890D gas chromatograph equipped with a thermal conductivity detector. Two columns were used in the analysis: Porapak QS and Molecular Sieve 5 Å. The total volumetric flowrate of the non-condensable components was measured with a bubble-soap meter.

Before the reaction tests, catalysts were reduced in situ at 600 °C for 1 h with 10% H_2/N_2 followed by purge with pure N_2 for 30 min.

The experiments were conducted at a constant pressure of 1.2 bar_a and temperatures ranging between 400 and 600 °C. The liquid feed flowrate was 1 ml/h for powder samples and it was varied between 1 and 15 ml/h for the metallic structures. The reactants composition at the reactor inlet was maintained constant for all experiences. N_2 was dosed to amount 37% molar in feed, while the inlet molar composition of ethanol and water were 9 and 54%, respectively. For the powder catalyst experiences, the nitrogen flowrate was set in 10 ml/min, with a total reactants flowrate of 27 ml/min. In the case of the catalytic plates, the nitrogen flowrate was varied in the range 10–150 ml/min, while the total flowrate at the reactor inlet was varied between 27 and 400 ml/min in order to maintain a constant composition.

For the evaluation of the carbon formation rate in the powder catalyst, 30 mg of Ni/CeMg sample were diluted on 150 mg of quartz particles and disposed into a fixed bed reactor. After reduction, the reaction test was conducted at 600 °C for 4.5 h with a liquid feed flowrate of 1 ml/h (S/C = 3).

The conversion of ethanol to C1 gaseous products was calculated using the following equation

$$X_{EtOH} = \frac{F_{CO} + F_{CO_2} + F_{CH_4}}{2 * F_{EtOH,in}} * 100 \quad (1)$$

where F are the molar flowrates of reactants and products. The gas phase products selectivity was calculated according to

$$S_i(\%) = \frac{F_i}{\sum F_i} * 100 \quad (2)$$

in which F_i refers to the molar flowrates of the reaction products.

Gas Hourly Space Velocity (GHSV) was calculated as the ratio of ethanol vapor flowrate at the reactor inlet (cm^3/h) to catalyst mass (g).

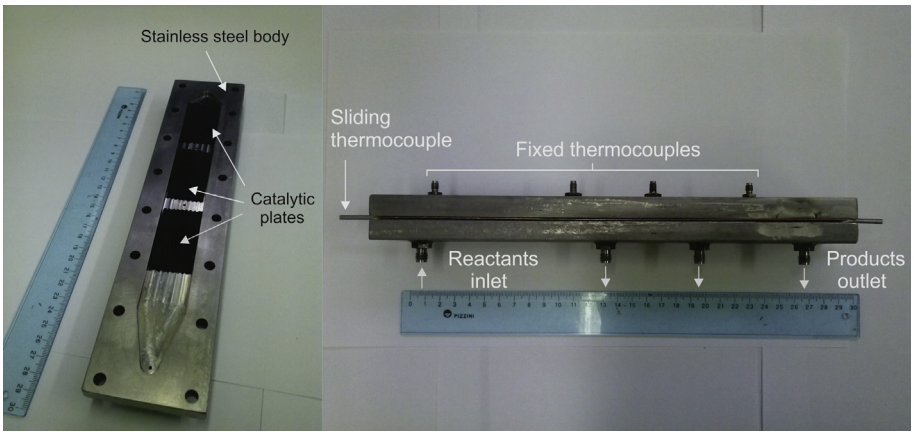

Fig. 1 – Stainless steel reactor photograph.

Results and discussion

Catalyst characterization

XRD profiles of the prepared catalysts are shown in Fig. 2A. In the support CeMg, the signals corresponding to the different planes of the cubic fluorite structure of CeO_2 are identified. The peeks corresponding to magnesium oxide could not be observed. This could obey to the fact that the MgO is well dispersed in the cerium oxide. Moreover, a small quantity of MgO may form a solid solution with CeO_2 [22]. The cerium oxide in the CeO_2–MgO support (CeMg) presented an average crystallite size of 12 nm as calculated by applying the Scherrer's equation to the (2,2,0) crystal plane peak, size that was confirmed by TEM (see below). The crystallite size for pure CeO_2 was 20.5 nm, which is higher than the crystal size calculated for the CeMg sample. This indicates that MgO inhibits the growth of CeO_2 crystals during the calcination process [23].

Fig. 2D shows the (111) and (200) reflections corresponding to CeO_2 fluorite structure for the pure CeO_2 and for the CeMg sample. The addition of Mg to the CeO_2 support did not produce an appreciable shift in the peaks corresponding to the cerium oxide. This means that a small incorporation of the Mg^{2+} cations into the cerium oxide structure took place for our synthesis conditions. The calculated lattice parameter of CeO_2 for both samples was very similar, 5.4082 Å for CeO_2 and 5.4080 Å for CeMg, which is in line with the previous observation.

The diffractogram of the catalyst Ni/CeMg show the appearance of the phase $Ni_xMg_{1-x}O$. The solid solution $Ni_xMg_{1-x}O$ is formed due to the strong interaction between Ni and the MgO of the support [20,24]. A major proportion of the Ni is found to take part of this solid solution; the rest is present as NiO [19]. A magnification of the $2\theta = 35–45°$ region of the Ni/CeMg catalyst is presented in Fig. 2B, where the positions of the MgO and NiO peaks as well as those of the $Ni_xMg_{1-x}O$ mixed oxide are indicated. The peak of the latter specie is located at an intermediate angle between those observed for the magnesium and nickel oxides, suggesting the incorporation of Ni^{2+} into the MgO structure after the calcination step and the formation of the $Ni_xMg_{1-x}O$ solid solution. A shift toward higher angles respect to MgO peaks has been reported as an evidence of the NiO–MgO solid solution formation [25]. The NiO diffraction peaks were located at 2θ values slightly higher than those presented by the mixed oxide, thus the overlapping made difficult a clear identification.

After Ni incorporation the position of CeO_2 peaks remained without noticeable modification indicating the absence of solid solutions with Ni. This fact is in accordance with the already reported limited solubility of NiO in the ceria lattice [26,27]. Nevertheless, it's worth mentioning that the occurrence of the solid solution depends also from the synthesis method and the subsequent treatments [28,29].

After the support deposition and Ni impregnation over the corrugated AISI-430 metallic carriers, the same signals as presented by the powdered Ni/CeMg catalyst were observed, indicating the presence of the same phases in the prepared structured catalyst.

After reaction, a broad band between $2\theta = 20–30°$ appeared, characteristic feature of amorphous carbon [30] (see Fig. 2C).

The catalyst composition of powder and coated plates are shown in Table 1. The composition was similar for the supported and particulate catalysts, with a greater amount of cerium in the support in the case of the coated plate. The latter sample also showed a slightly higher concentration of nickel. The specific surface area did not significantly change after the deposition process, being of 28.21 m^2/g for the Ni/CeMg powder catalyst and 29.82 m^2/g for the SS-Ni/CeMg plate.

TEM images of the fresh samples and catalysts after 6 h on-stream at 600 °C are reported in Fig. 3. Nanometric-size crystals can be observed with a mean particle diameter ranging 10–15 nm. After ESR, the appearance of carbon filaments is observed in certain regions of the catalyst surface (see Fig. 3C). Carbon atoms formed over the Ni particles move by surface diffusion and nucleate in the back side of the crystals giving rise to the filament [18]. The growth of this structures leads to the detachment of the metallic particles, which loss the contact with the support. The formation of these hollowed filaments [31,32] did not lead to an observable catalyst deactivation, in agreement with previous reports in the literature [33]. This fact suggests that the main source of carbon

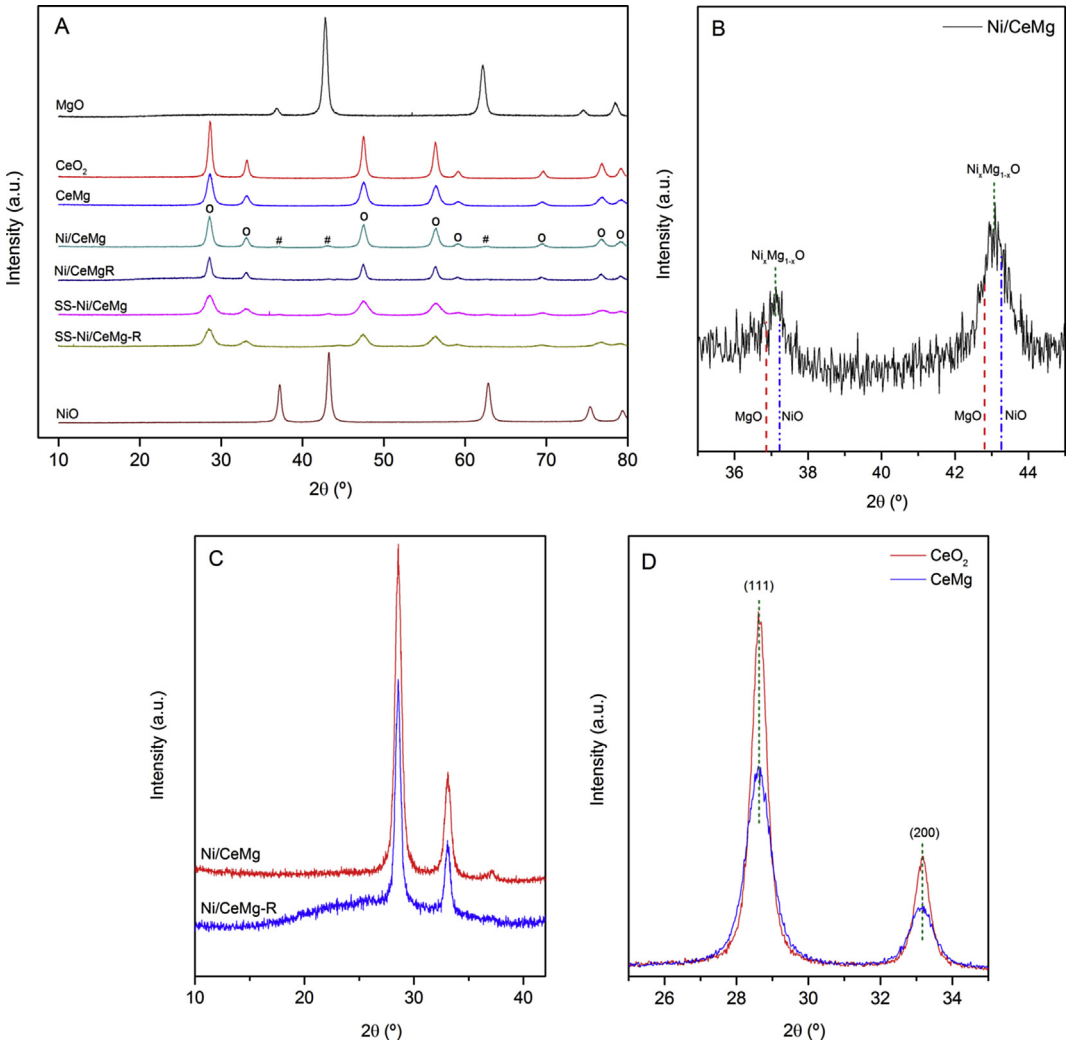

Fig. 2 – A) XRD patterns of the powder and structured catalysts, B) Magnification of the 2θ = 35–45° region of the Ni/CeMg catalyst, C) Magnification of the 2θ = 10–45° region of the fresh Ni/CeMg catalysts and the same sample after reaction, D) Detail of the (111) and (200) cerium oxide peaks for the CeO_2 and CeMg diffractograms. Ref.: (o) CeO_2, (#) $Ni_xMg_{1-x}O$.

deposition over this catalytic system follows the mentioned path. On the other hand, Zhang et al. [20] evaluated the rate of carbon deposition over Ni/MgO–CeO_2 catalysts in ethanol steam reforming at 400 °C using a catalyst weight-to-ethanol flowrate of W/F = 33 g h/mol. They observed that the rate of carbon deposition varied from about 15 $mg_C/(g_{cat}$ h) to 2 $mg_C/(g_{cat}$ h) for a constant 10% Ni loading and varying the Mg molar fraction in the support from 10 mol% to 50 mol%. In our case, for the powder catalyst with an intermediate Mg concentration of 15 mol% tested under slightly more severe conditions (600 °C and W/F = 4.6 g h/mol), a rate of 13.9 $mg_C/(g_{cat}$ h) was observed, indicating that the catalyst performed satisfactorily with a rate of carbon formation according to literature.

The catalytic plates were analyzed by scanning electron microscopy, the micrographs corresponding to the SS-Ni/CeMg samples are presented in Fig. 4. The thickness of the deposited catalytic layer was approximately 25 μm (see Fig. 4C). The plates exhibited mechanical integrity after the reaction tests. As in the case of powder catalysts, carbon formation also took place on the catalytic plates, particularly at the inlet region of these structures. The plate surface observed by SEM presented similar features before and after the

Table 1 – Composition of the powder and structured catalysts.

Sample	Type of catalyst	Ce/(Ce + Mg) molar ratio	Mg/(Ce + Mg) molar ratio	Ni wt.%	$SiO_2/(CeO_2–MgO)$[a]
CeMg	Powder	0.87	0.13	–	–
Ni/CeMg	Powder	0.85	0.15	7	–
SS-Ni/CeMg	Structured	0.92	0.08	10	0.10

[a] Nominal composition, expressed in g_{SiO_2} per $g_{support}$.

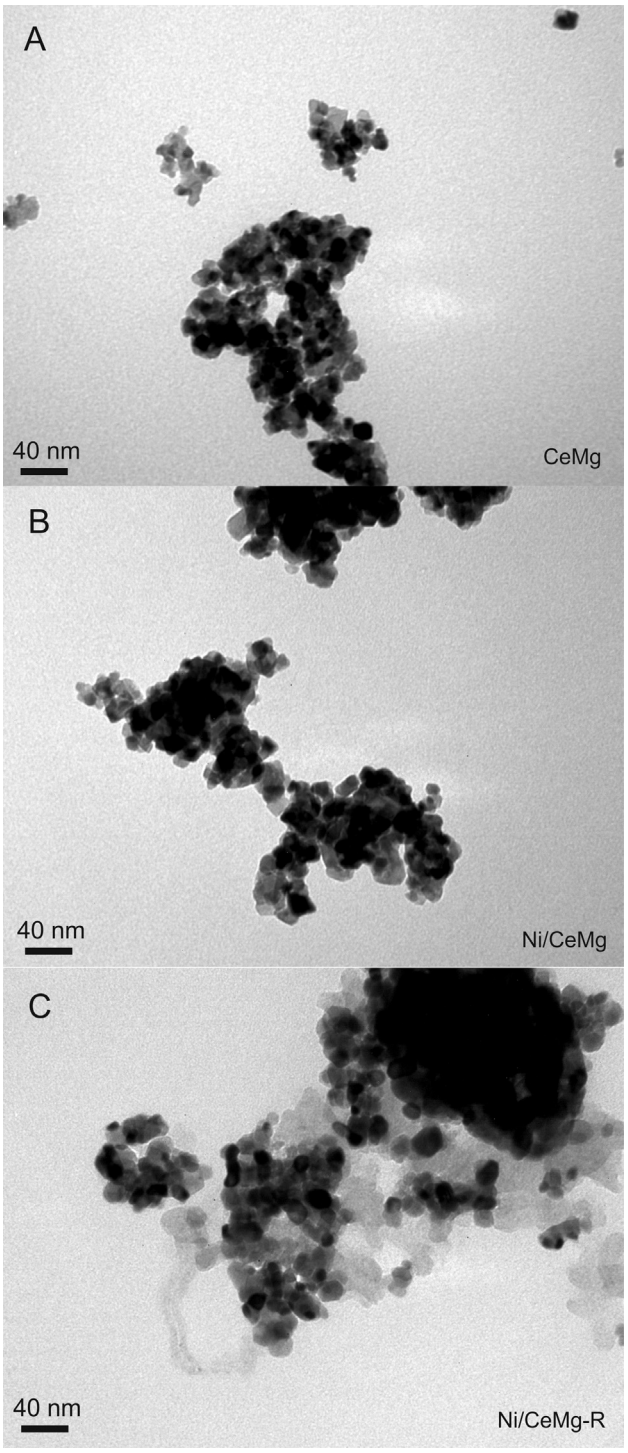

Fig. 3 – TEM images of the A) CeO_2–MgO support, B) Ni/CeMg sample and C) Ni/CeMg after ESR reaction.

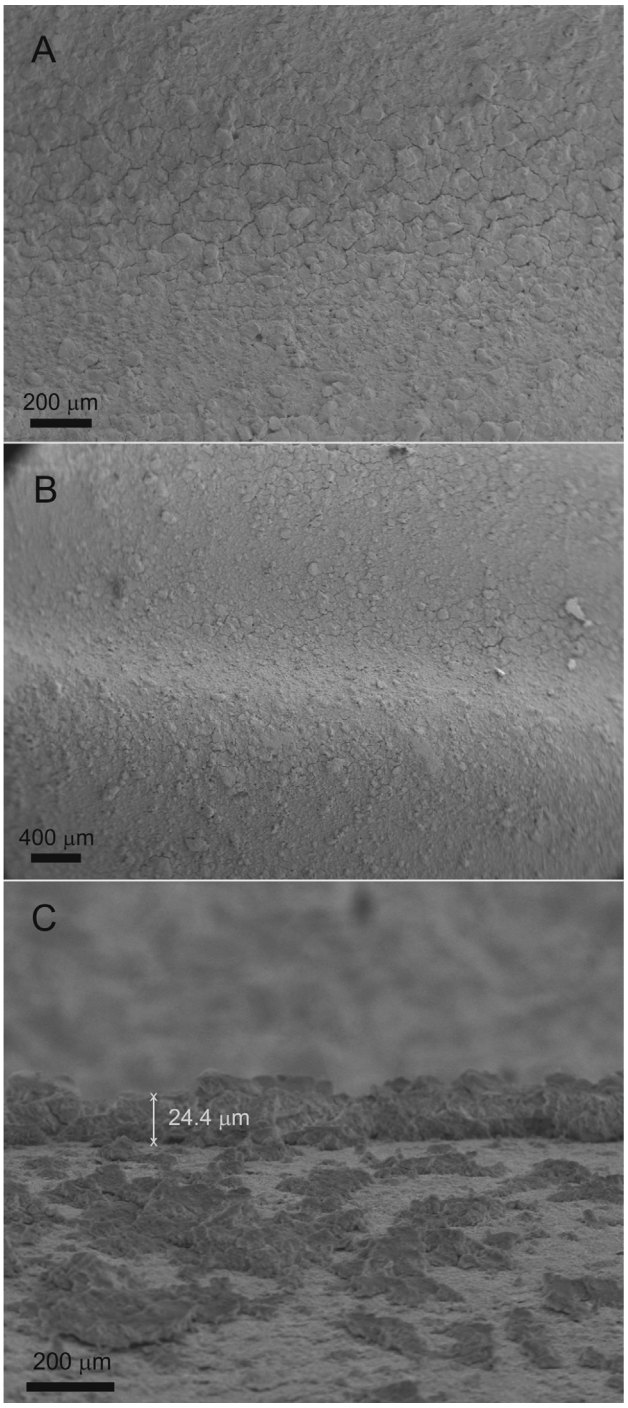

Fig. 4 – SEM micrographs of catalytic plates A) fresh B) after 10 h on-stream at 600 °C. C) Cross-section of the deposited coating.

reaction test (Fig. 4A and B, respectively). The resistance against the coating detachment can be attributed mainly to the colloidal silica addition. This inorganic binder was used to increase the coating adherence and to improve the stability of the catalytic suspension for the washcoating procedure. SiO_2 particles are roughly two orders of magnitude smaller in size than the catalyst particles. During the drying step, the small particles are drawn by capillary forces at the contact points of the larger catalyst particles, increasing the surface of contact and enhancing the mechanical anchorage [14,34].

The TPR profiles of cerium oxide and the nickel catalysts are shown in Fig. 5. CeO_2 presented a broad reduction peak in the temperature range selected for the analysis, with a maximum centered at 450 °C. This signal is attributed to the reduction of the CeO_2 surface oxygen.

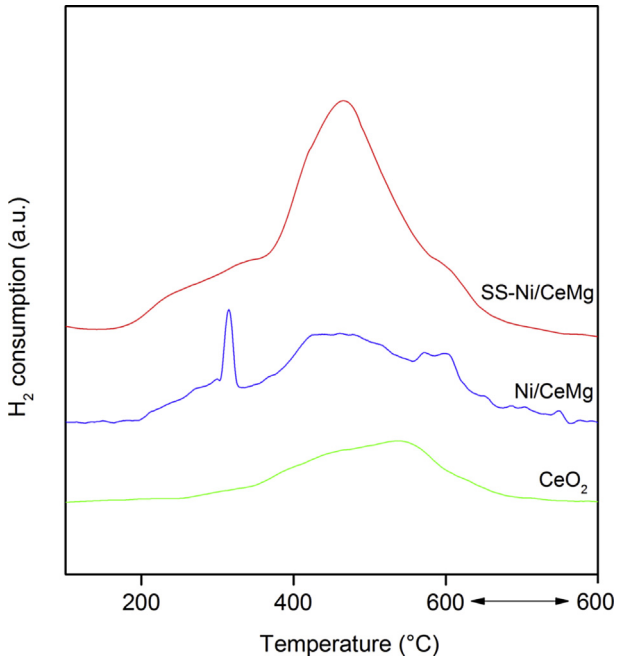

Fig. 5 – TPR profiles of cerium oxide and the Ni-loaded catalysts.

For Ni-loaded samples, it was observed that the onset of the reduction occurred at temperatures lower than those presented by pure CeO_2, possibly due to the reduction of surface non-stoichiometric Ni^{3+} species [35]. Ni/CeMg catalyst shows a hydrogen consumption peak centered at 315 °C, indicating the reduction of bulk nickel oxide [36]. It is interesting to note that this peak is not observed in the SS-Ni/CeMg reduction profile. This is probably due to a higher interaction of nickel oxide with CeO_2 [37], leading to an increase in the reduction temperature (up to 470 °C for ceria-supported Ni catalysts [38]) and a overlapping of the Ni^{2+} reduction peak with that corresponding to CeO_2 surface oxygen.

The oxygen storage capacity complete of the Ni/CeMg catalyst, CeMg support and reference materials are presented in Table 2. The amount of oxygen stored by the CeMg support is lower than the OSCC of undoped ceria. This could be a consequence of the very small incorporation of Mg into the cerium oxide structure. It is known that the substitution of Ce^{4+} by a metal ion with a lower valence creates oxygen vacancies to maintain the charge balance in the ceria lattice, increasing consequently the OSC of CeO_2 [39]. The Mg-promoted ceria prepared in the present work presented an OSCC between the values observed for CeO_2 and MgO, suggesting that Mg is present in a segregated phase instead of incorporated in the ceria lattice, as the oxygen consumption in the CeMg sample roughly corresponds to the sum of MgO and CeO_2 pure oxide contributions. These results are in agreement with the XRD data, in which it was not evidenced a significant modification in the lattice parameters of CeO_2 after the addition of Mg for the synthesis conditions of the CeMg support.

Table 2 – Oxygen storage capacity complete of the Ni-loaded catalyst, CeMg support and reference materials at 400 °C.

	CeO_2	MgO	CeMg	Ni/CeMg
OSCC, μmol CO_2 g^{-1}	490	192	356	1267

OSCC of Ni/CeMg is considerably higher than those presented by CeMg. The additional OSC observed in the nickel-loaded sample respect to the CeMg support exceeds the amount of oxygen stored by Ni. The latter oxygen amount corresponds to the reduction of Ni^{2+} into Ni°, and it was evaluated considering that only a fraction of the nickel in the catalyst can be reduced under the conditions of the analysis due to the formation of the $Ni_xMg_{1-x}O$ solid solution, according to previous studies in literature for catalysts with the same composition of Ni/CeMg [20]. A reasonable explanation for this phenomenon could be that part of the oxygen is stored on the support assisted by Ni [40].

Catalytic tests

Powder catalyst

Fig. 6 shows the catalytic performance of the Ni/CeMg powder in the ESR reaction at different temperatures.

When operation at low temperatures is selected (e.g., T = 427 °C) the main reaction observed is the dehydrogenation of ethanol to render acetaldehyde (equation (Rx1)), which consecutively decomposes to give equal quantities of methane and carbon monoxide (eq. (Rx2)). Reaction (Rx1) has been already reported for catalysts containing Ni [21,41–44]. The presence of acetaldehyde was detected here at low temperatures (not shown in Fig. 6); only traces were found for T > 475 °C. Molar ratio CO:CH_4 of 1:1 until ca. 550 °C point to the occurrence of acetaldehyde decomposition; temperatures higher than 550 °C show increasing levels of methane steam reforming (see eq. (Rx3)) approaching equilibrium values. In fact, the use of CeO_2 promotes methane reforming due to the

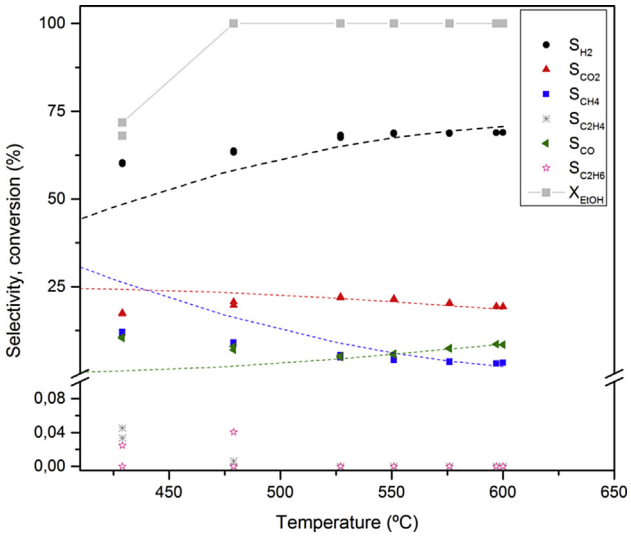

Fig. 6 – Ethanol steam reforming tests of the powder catalyst at different temperatures. Reaction conditions: S/C = 3, GHSV = 4895 $cm^3/g_{cat}/h$ (W/F = 0.735 g s/cm^3). Dashed lines represent equilibrium compositions.

presence of oxygen vacancies which enhances H_2 and CO_2 selectivities [19]. At higher temperatures (550 < T < 600 °C), thermodynamic constraints favor the build-up of CO at expenses of CO_2 via the reverse water–gas shift reaction (Rx4), which is essentially in equilibrium at these temperature levels [45,46]. For temperatures below 450 °C, it was observed an incomplete ethanol conversion to C_1 gaseous products, accompanied by the presence of acetaldehyde, small amounts of ethylene, ethane and the unconverted ethanol.

$$C_2H_5OH \rightarrow C_2H_4O + H_2 \quad \text{(Rx1)}$$

$$C_2H_4O \rightarrow CO + CH_4 \quad \text{(Rx2)}$$

$$CH_4 + H_2O \leftrightarrow CO + 3H_2 \quad \text{(Rx3)}$$

$$CO + H_2O \leftrightarrow CO_2 + H_2 \quad \text{(Rx4)}$$

$$C_2H_4O + 3H_2O \rightarrow 2CO_2 + 5H_2 \quad \text{(Rx5)}$$

The stability of the prepared catalyst was evaluated by means of an 18 h on-stream reaction test in which the powder sample was subjected to ESR at 600 °C (Fig. 7). The catalyst showed constant activity values with a products distribution that remained unaltered at the initial levels along the whole experience.

The carbon balance in the absence of condensable products varied around ±10% for the powder and structured catalysts. This condition was observed at temperatures higher than 475 °C for the powder catalyst and space velocities lower than 5000 $cm^3/g_{cat}/h$ in the case of the catalytic plates.

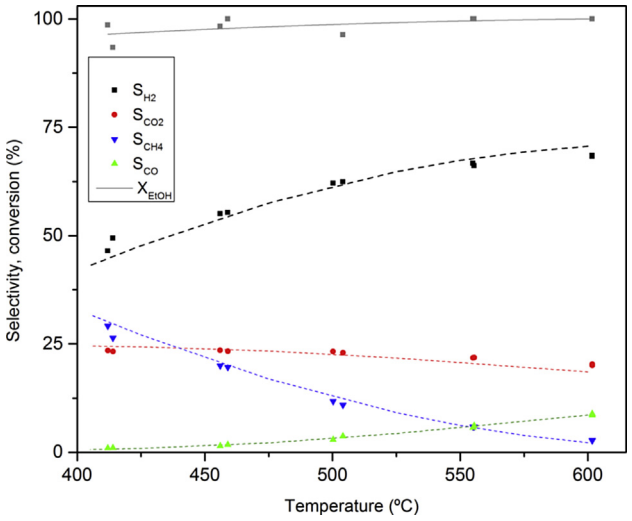

Fig. 8 – Influence of the temperature over the performance of the structured catalyst under ESR. Reaction conditions: S/C = 3, GHSV = 316 $cm^3/g_{cat}/h$. Dashed lines represent equilibrium compositions.

Catalytic plates

The AISI-430 structured catalysts were tested towards H_2 generation via the ethanol steam reforming reaction. In line with the previous discussion in Section "Catalyst characterization" emphasizing the similarity between the catalytic material deposited on the metallic corrugated supports and the powder catalyst, the structured catalysts show the same behavior as the powder catalyst under reaction conditions, presenting high activity and adequate selectivity to H_2 (see Fig. 8).

Under the conditions adopted for the experiences, ethanol conversions close to 100% were achieved along the whole

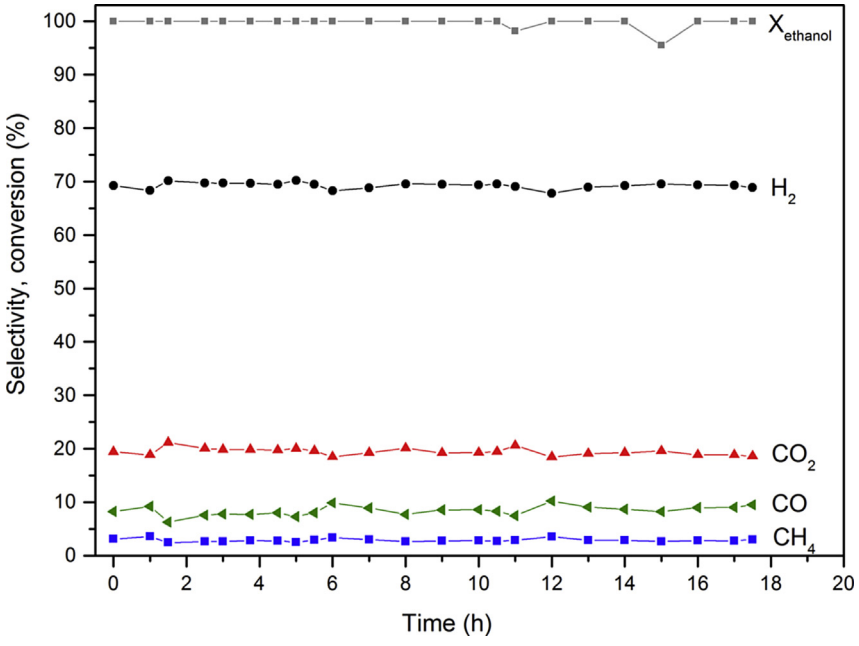

Fig. 7 – Stability test for ESR for the powder catalyst. Reaction conditions: T = 600 °C, S/C = 3, GHSV = 4895 $cm^3/g_{cat}/h$ (W/F = 0.735 g s/cm^3).

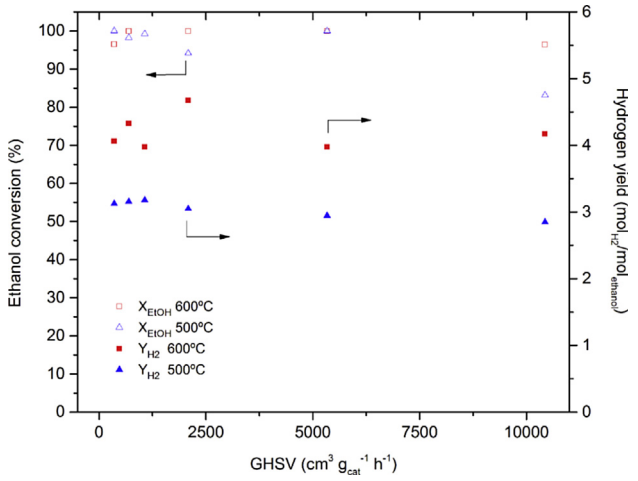

Fig. 9 – Ethanol steam reforming tests of the structured catalyst at different feed flowrates. Reaction conditions: S/C = 3, T = 500–600 °C, GHSV = 356–10,432 cm^3/g$_{cat}$/h.

temperature range. Regarding the products distribution and based on the selection of a reduced value of GHSV, equilibrium compositions were achieved even at the lowest reaction temperature tested. Here, higher residence times allow the evolution of CO towards CH_4 (reverse of eq. (Rx3), i.e., methanation) once acetaldehyde has decomposed, as already discussed for Fig. 6.

The catalytic performance of the catalytic plates was evaluated at different feed flowrates. Fig. 9 shows the conversion of ethanol and H_2 yield at different space velocities and temperatures. At 600 °C, both complete ethanol conversion and a H_2 yield of 4.2 $mol_{H_2}/mol_{ethanol}$ remained practically constant with increasing GHSV. Conversely, for the experiences conducted at 500 °C it was observed for the highest space velocity (10,432 cm^3/g$_{cat}$/h) a drop in the conversion of ethanol, accompanied by a reduction of the H_2 yield. These feed conditions indicate an operative limit, after which the catalytic performance of the catalyst decreases significantly.

As shown in Fig. 10, measured selectivities correspond to equilibrium values, regardless of the selected space velocity. Unlike powder catalysts, ethane and ethylene were not detected for all experiments over the structured catalysts. The departure from equilibrium conditions at 500 °C and the highest GHSV was also evidenced in the products distribution, where an increase in H_2 and CO selectivities was observed, along with a lower selectivity to CH_4 and CO_2. A similar behavior was observed for the powder sample at the same temperature, where selectivities shifted away from equilibrium values in the same way (i.e., the CO and CH_4 selectivities tend to the same value and hydrogen selectivity appears above the equilibrium line). This fact indicates that the catalytic material performs equivalently before and after being deposited on the metal substrate.

For the powder catalyst, the product selectivities at T < 525 °C experienced a slight departure from the equilibrium conditions, as shown in Fig. 5. In the case of the catalysts supported on steel plates, the products distribution was found to be almost at equilibrium levels at the same temperature and space velocity (T = 500 °C and GHSV = 4895 cm^3/g$_{cat}$/h). This slightly higher activity exhibited by the plates respect to the powder catalyst could be attributed to the higher Ni content in the plates, according to the chemical analysis (see Table 1). According to literature reports on supported nickel catalysts, the increase in Ni loading leads to an increase in ethanol steam reforming activity [47,48].

Other important observation is that the addition of SiO_2 did not show a detrimental effect on the catalytic performance. It is known that the use of inorganic additives such as silica favors the mechanical anchoring of the covering to the support and improves the suspensions stability, but it can also modify the catalytic properties of the deposited material [14].

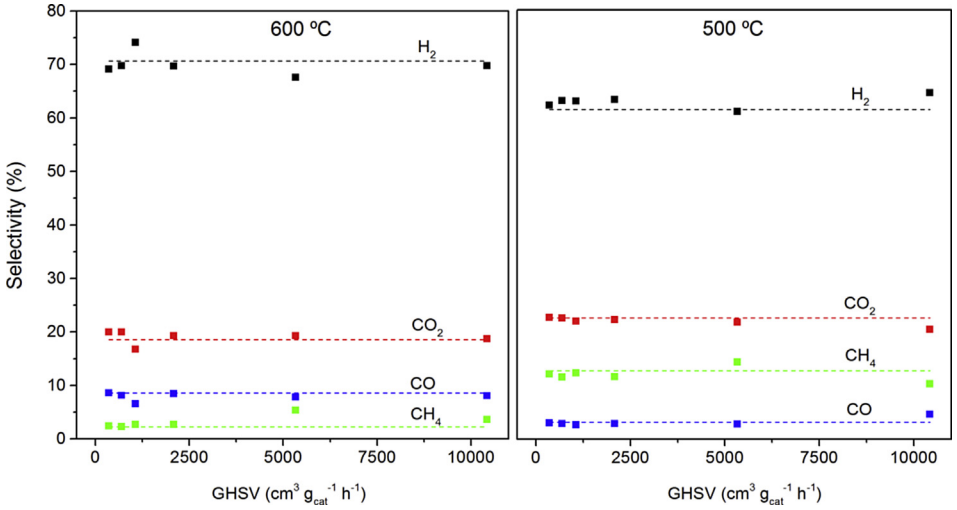

Fig. 10 – Products distribution in ethanol steam reforming tests over the structured catalyst at different feed flowrates and temperatures. Reaction conditions: S/C = 3, T = 500 °C and T = 600 °C, GHSV = 356–10,432 cm^3/g$_{cat}$/h. Dashed lines indicate equilibrium selectivities.

The supports having redox properties (e.g. CeO_2) show enhanced ESR performance since they favor the coke removal [49], and specially cerium oxide has the capacity to activate H_2O molecules, producing oxygen species that can oxidize reaction intermediates adsorbed on the catalyst surface to form H_2 and CO_2 [20]. As mentioned in the present work, it was not observed a decrease in the ethanol conversion or H_2 selectivity attributed to the presence of silica.

From the point of view of the reactor operation, supporting the Ni/CeMg catalysts on corrugated steel plates allowed to work with high GHSV values with a very low pressure drop (<1 psi), which was not possible with the powder catalyst even at the lowest flowrate. Moreover, the use of metallic substrates provides more uniformity in the temperature profiles of the plates and the higher open areas given by the structured catalysts leads to a lower tendency to plugging by carbon deposition.

Conclusions

Both Ni/CeO_2–MgO catalysts in powder form and supported on stainless steel plates were prepared, characterized and tested in the ethanol steam reforming reaction. The coatings obtained were homogeneous and retained its integrity after the reaction experiences.

Catalysts presented a very good stability under reaction conditions for 16 h, without showing a significant variation in the activity or product distribution. Hydrogen yields of 4.2 $mol_{H_2}/mol_{ethanol}$ were achieved for the structured catalysts operating at 600 °C with a GHSV of 10,432 $cm^3/g_{cat}/h$, rendering a hydrogen production of 103 ml_{STP} H_2/cm^3 of structured catalyst.

Structured catalysts presented similar activities and selectivities when compared to those of the powder, concluding that the deposition method do not modify the catalytic properties of the particulate material. On the other hand, the addition of SiO_2 as a binder to the catalytic suspensions did not lead to a drop in the ethanol conversion level and the products selectivities remained unchanged. The presence of the metallic substrate did not show any influence in the catalytic performance as well. The latter fact points AISI 430 stainless steel corrugated plates as suitable substrates for conducting the ethanol steam reforming reaction.

The possibility of selecting metallic structured catalysts instead of powder allowed working with elevated values of GHSV with neglectable pressure drops while providing enhanced heat transfer capabilities and reducing the tendency to plugging due to coke deposition.

Acknowledgments

The authors thank the Agencia Nacional de Promoción Científica y Tecnológica (National Agency of Scientific and Technological Promotion, Argentina), the Consejo Nacional de Investigaciones Científicas y Técnicas (National Council for Scientific and Technological Research) and the Universidad Nacional del Sur for the financial support.

REFERENCES

[1] Chaubey R, Sahu S, James OO, Maity S. A review on development of industrial processes and emerging techniques for production of hydrogen from renewable and sustainable sources. Renew Sustain Energy Rev 2013;23:443–62.
[2] Ni Meng, Leung DYC, Leung MKH. A review on reforming bio-ethanol for hydrogen production. Int J Hydrogen Energy 2007;32:3238–47.
[3] Hou T, Zhang S, Xu T, Cai W. Hydrogen production from oxidative steam reforming of ethanol over Ir/CeO_2 catalysts in a micro-channel reactor. Chem Eng J 2014;255:149–55.
[4] Goyal N, Pant KK, Gupta R. Hydrogen production by steam reforming of model bio-oil using structured Ni/Al_2O_3 catalysts. Int J Hydrogen Energy 2013;38:921–33.
[5] Casanovas A, Domínguez M, Ledesma C, López E, Llorca J. Catalytic walls and micro-devices for generating hydrogen by low temperature steam reforming of ethanol. Catal Today 2009;143:32–7.
[6] Heck RM, Gulati S, Farrauto RJ. The application of monoliths for gas phase catalytic reactions. Chem Eng J 2001;82:149–56.
[7] Cybulski A, Moulijn JA. Structured catalysts and reactors. New York: Marcel Dekker; 1998.
[8] Jensen KF. Microreaction engineering – is small better? Chem Eng Sci 2001;56:293.
[9] Llorca J, Casanovas A, Trifonov T, Rodríguez A, Alcubilla R. First use of macroporous silicon loaded with catalyst film for a chemical reaction: a microreformer for producing hydrogen from ethanol steam reforming. J Catal 2008;255:228–33.
[10] Ehrfeld W, Hessel V, Löwe H. Microreactors: new technology for modern chemistry. Weinheim: Wiley-VCH Verlag GmbH; 2000.
[11] Kolb G. Review: microstructured reactors for distributed and renewable production of fuels and electrical energy. Chem Eng Process 2013;65:1–44.
[12] Sanz O, Echave FJ, Romero-Sarria F, Odriozola JA, Montes M. Advances in structured and microstructured catalytic reactors for hydrogen production. In: Gandia LM, Arzamedi G, Dieguez PM, editors. Renewable hydrogen technologies: production, purification, storage. Applications and Safety, Elsevier B.V.; 2013. p. 201–24.
[13] López E, Irigoyen A, Trifonov T, Rodríguez A, Llorca J. A million-channel reformer on a fingertip: moving down the scale in hydrogen production. Int J Hydrogen Energy 2010;35:3472–9.
[14] Avila P, Montes M, Miró Eduardo E. Monolithic reactors for environmental applications: a review on preparation technologies. Chem Eng J 2005;109:11–36.
[15] Amuda MOH, Mridha S. Microstructural features of AISI 430 ferritic stainless steel (FSS) weld produced under varying process parameters. Int J Mech Mater Eng 2009;4:160–6.
[16] Santander JA, Lopez E, Tonetto GM, Pedernera MN. Preparation of NiNbO/AISI 430 ferritic stainless steel monoliths for catalytic applications. Ind Eng Chem Res 2014;53:11312–9.
[17] Gates SM, Russell JN, Yates JT. Bond activation sequence observed in the chemisorption and surface reaction of ethanol on Ni (111). Surf Sci 1986;171:111–34.
[18] Sehested Jens. Four challenges for nickel steam-reforming catalysts. Catal Today 2006;111:103–10.
[19] Cai W, Wang F, Zhan E, Van Veen AC, Mirodatos C, Shen W. Hydrogen production from ethanol over Ir/CeO_2 catalysts: a comparative study of steam reforming, partial oxidation and oxidative steam reforming. J Catal 2008;257:96–107.

[20] Zhang C, Li S, Li M, Wang S, Ma X, Gong J. Enhanced oxygen mobility and reactivity for ethanol steam reforming. AIChE J 2012;58:516–25.
[21] Zhuang Q, Qin Y, Chang L. Promoting effect of cerium oxide in supported nickel catalyst for hydrocarbon steam-reforming. Appl Catal 1991;70:1–8.
[22] Osaka M, Serizawa H, Kato M, Naka Jima K, Tachi Y, Kitamura R, et al. Research and development of minor actinide-containing fuel and target in a future integrated closed cycle system. J Nucl Sci Technol 2007;44:309–16.
[23] Chen J, Zhu J, Zhan Y, Lin X, Cai G, Wei K, et al. Characterization and catalytic performance of Cu/CeO_2 and $Cu/MgO\text{-}CeO_2$ catalysts for NO reduction by CO. Appl Catal A Gen 2009;363:208–15.
[24] Parmaliana A. Temperature-programmed reduction study of NiO-MgO interactions in magnesia-supported Ni catalysts and NiO-MgO physical mixture. J Chem Soc Faraday Trans 1990;86:2663–9.
[25] Jafarbegloo M, Tarlani A, Wahid Mesbah A, Muzart J, Sahebdelfar S. NiO–MgO solid solution prepared by sol–gel method as precursor for Ni/MgO methane dry reforming catalyst: effect of calcination temperature on catalytic performance. Catal Lett 2016;146:238–48.
[26] Mogensen M, Sammes NM, Tompsett GA. Physical, chemical and electrochemical properties of pure and doped ceria. Solid State Ionics 2000;129:63–94.
[27] Solak N. Interface stability in solid oxide fuel cells for intermediate temperature applications [Dissertation]. Max-Planck-Institut für Metallforschung Stuttgart; 2007.
[28] Romero-Núñez A, Díaz G. High oxygen storage capacity and enhanced catalytic performance of $NiO/Ni_xCe_{1-x}O_2$-nanorods: synergy between Ni-doping and 1D morphology. RSC Adv 2015;5:54571–9.
[29] Liu X, Zuo Y, Li L, Huang X, Li G. Heterostructure $NiO/Ce_{1-x}Ni_xO_2$: synthesis and synergistic effect of simultaneous surface modification and internal doping for superior catalytic performance. RSC Adv 2014;4:6397–406.
[30] Yang X, Li C, Wang W, Yang B, Zhang S, Qian Y. A chemical route from PTFE to amorphous carbon nanospheres in supercritical water. Chem Commun 2004;3:342–3.
[31] Baker RTK, Barber MA, Harris PS, Feates FS, Waite RJ. Nucleation and growth of carbon deposits from the nickel catalyzed decomposition of acetylene. J Catal 1972;26:51–62.
[32] Helveg S, Sehested J, Rostrup-Nielsen JR. Whisker carbon in perspective. Catal Today 2011;178:42–6.
[33] Alberton AL, Souza MMVM, Schmal M. Carbon formation and its influence on ethanol steam reforming over Ni/Al_2O_3 catalysts. Catal Today 2007;123:257–64.
[34] Nijhuis TA, Beers AEW, Vergunst T, Hoek I, Kapteijn F, Moulijn JA. Preparation of monolithic catalysts. Catal Rev Sci Eng 2001;43:345–80.
[35] Frusteri F, Freni S, Chiodo V, Donato S, Bonura G, Cavallaro S. Steam and auto-thermal reforming of bio-ethanol over MgO and CeO_2 Ni supported catalysts. Int J Hydrogen Energy 2006;31:2193–9.
[36] Zhang B, Tang X, Li Y, Cai W, Xu Y, Shen W. Steam reforming of bio-ethanol for the production of hydrogen over ceria-supported Co, Ir and Ni catalysts. Catal Commun 2006;7:367–72.
[37] Shi Q, Liu C, Chen W. Hydrogen production from steam reforming of ethanol over $Ni/MgO\text{-}CeO_2$ catalyst at low temperature. J Rare Earths 2009;27:948–54.
[38] Zhang C, Li S, Wu G, Gong J. Synthesis of stable $Ni\text{-}CeO_2$ catalysts via ball-milling for ethanol steam reforming. Catal Today 2014;233:53–60.
[39] Cho BK. Chemical modification of catalyst support for enhancement of transient catalytic activity: nitric oxide reduction by carbon monoxide over rhodium. J Catal 1991;131:74–87.
[40] Kacimi S, Barbier Jr J, Taha R, Duprez D. Oxygen storage capacity of promoted Rh/CeO_2 catalysts. Exceptional behavior of $RhCu/CeO_2$. Catal Lett 1993;22:343–50.
[41] Fatsikostas AN, Verykios XE. Reaction network of steam reforming of ethanol over Ni-based catalysts. J Catal 2004;225:439–52.
[42] Fajardo HV, Probst LFD, Carreño NLV, Garcia ITS, Valentini A. Hydrogen production from ethanol steam reforming over Ni/CeO_2 nanocomposite catalysts. Catal Lett 2007;119:228–36.
[43] Liberatori JWC, Ribeiro RU, Zanchet D, Noronha FB, Bueno JMC. Steam reforming of ethanol on supported nickel catalysts. Appl Catal A Gen 2007;327:197–204.
[44] Zanchet D, Santos JB, Damyanova S, Gallo JMR, Bueno JMC. Towards understanding metal-catalyzed ethanol reforming. ACS Catal 2015;5:3841–63.
[45] Men Y, Kolb G, Zapf R, Hessel V, Löwe H. Ethanol steam reforming in a microchannel reactor. Trans IChemE Part B 2007;85:413–8.
[46] Patel M, Jindal TK, Pant KK. Kinetic study of steam reforming of ethanol on Ni-based ceria–zirconia catalyst. Ind Eng Chem Res 2013;52:15763–71.
[47] Biswas P, Kunzru D. Steam reforming of ethanol for production of hydrogen over $Ni/CeO_2–ZrO_2$ catalyst: effect of support and metal loading. Int J Hydrogen Energy 2007;32:969–80.
[48] Bshish A, Yaakob Z, Ebshish A, Alhasan FH. Hydrogen production via ethanol steam reforming over Ni/Al_2O_3 catalysts: effect of Ni loading. J Energy Resour Technol 2014;136:12601.
[49] Llorca J, Corberán VC, Divins NJ, Fraile RO, Taboada E. Hydrogen from bioethanol [Chapter 7]. In: Gandia LM, Arzamedi G, Dieguez PM, editors. Renewable hydrogen technologies: production, purification, storage, applications and safety. Elsevier; 2013. p. 135–69.